IAC–24–C1,6,4,x84151

A direct optimization approach for robust trajectories of interplanetary CubeSats

Carmine Giordano[a*], **Francesco Topputo**[b]

[a] *Department of Aerospace Science and Technology, Politecnico di Milano, via La Masa, 34, Milan, 20156, Italy, carmine.giordano@polimi.it*
[b] *Department of Aerospace Science and Technology, Politecnico di Milano, via La Masa, 34, Milan, 20156, Italy, francesco.topputo@polimi.it*
[*] *Corresponding author*

Abstract

Nowadays, the space exploration is going in the direction of exploiting small platforms to get high scientific return at significantly lower costs. However, miniaturized spacecraft pose different challenges both from the mission analysis point of view. Nominal trajectories of traditional spacecraft are designed and optimized in order to satisfy only scientific requirements as well as to comply with system constraints. Although, the nominal path will unlikely be followed by the spacecraft in real-life scenarios due to uncertainty in dynamic model, navigation, and command actuation, the correction maneuvers needed to compensate deviations are considered to be a minor problem, since changing the trajectory is relatively easy with a single, short burn. Robustness and feasibility assessment of the nominal trajectory against uncertainty are performed a-posteriori. Thus, the nominal trajectory and the uncertainty assessment are decoupled and their analysis and optimization are done in two separate phases. This approach can lead to sub-optimal solutions. For large spacecraft, this procedure is acceptable since they can produce high thrust levels and they can store relevant propellant quantities; hence, sub-optimal trajectories are not critical. However, small platforms are characterized by low control authority, that poses challenges in maneuvering. Therefore, correction maneuvers cannot be considered a minor problem and preliminary trajectory design should take them into account. To solve this problem, in this work, a direct optimization method is devised to design robust trajectories for interplanetary small spacecraft. The robust optimal control problem is translated in a nonlinear programming problem by means of transcription and collocation, while a linearized approach is exploited to propagate and quantify all the uncertainties related to unmodeled perturbations, imperfect knowledge of the state, and control application. This methodology has been than applied to the interplanetary transfer of the CubeSat M-ARGO, that is planned to be the first standalone ESA deep-space CubeSat to rendezvous a near-Earth asteroid. This new technique is able to bring a 50% save in the navigation costs, while being able to rendezvous the target asteroid with great accuracy.

1. Introduction

The trajectory design process for spacecraft has traditionally prioritized scientific goals and system constraints, relying on the robust capabilities of chemical propulsion systems. These propulsion systems, known for delivering high thrust and providing strong control authority, have long enabled spacecraft to adjust their paths with relative ease. In standard practice, nominal trajectories are optimized under the assumption that minor deviations can be corrected with brief, high-thrust maneuvers. This approach assumes that any uncertainties in the mission, whether due to dynamic models (such as gravitational variations or unpredictable solar radiation pressure), navigation inaccuracies, or errors in command execution [1], can be managed in a separate, later phase of the mission design. After the nominal trajectory is established, a post-design phase assesses the robustness and feasibility of the trajectory, estimating the necessary correction maneuvers and the achievable accuracy of the spacecraft state. This sequential, decoupled approach generally leads to acceptable outcomes for larger spacecraft, which have substantial thrust capabilities and significant propellant reserves. However, recently, there has been a growing focus on smaller platforms like SmallSats and CubeSats. These miniaturized spacecraft offer the potential for cost-effective missions, delivering scientific and technological benefits at a fraction of the traditional cost [2, 3]. However, their small size brings significant challenges, particularly in trajectory control. With limited propulsion systems that provide low thrust and skeletal propellant budgets, these spacecraft cannot afford the inefficiencies tolerated by larger vehicles. Moreover, they often operate under greater uncertainty due to less mature navigation techniques and the inherent limitations of miniaturized components, which introduce higher errors in both state estimation and command execution.

Given these constraints, the traditional approach to trajectory design, where nominal paths are optimized without fully integrating uncertainty considerations, is no longer sufficient. For miniaturized probes, trajectory corrections are not merely minor adjustments but critical operations that can significantly impact the mission success. Consequently, trajectory design for these platforms must integrate uncertainties from the outset, ensuring that the path selected is not only optimal under nominal conditions but also feasible and robust against uncertainties.

For this reason, in the last ten years, stochastic-optimal approaches, embedding uncertainty in their core, have been developed for diverse problems. In the early 2000, [4] proposed a statistical targeting algorithm, able to incorporate statistical information directly in the trajectory design. While the usual target method solves a deterministic boundary value problem for the nominal trajectory, this algorithm search for a statistically correct trajectory, i.e., a trajectory able to reach the target state in a stochastic sense. However this approach fails whenever the stochastic trajectories envelope cannot be described as a quasi-Gaussian distribution.

The uncertain Lambert's problem has been investigated alike by exploiting Taylor differential algebra [5–7]. An alternative approach, characterizing the stochastic error by means of the first-order variational equations, is presented in [8]. This approach has been extended considering first the explicit partial derivatives of the transfer velocities [9] and later by implementing a derivative free numerical method, exploiting novelties in uncertainty quantification [10]. Uncertain Lambert's problem with differential algebra was also exploited in the gravity assist space pruning algorithm presented in [11].

Similarly, approaches to tackle the rendezvous problem were conceived. A multi-objective optimization method, considering a robust performance index based on final uncertainties, was devised for the linear rendezvous problem [12], taking into account both navigation and control errors. A relation among the performance index, the rendezvous time, and the propellant cost was found for short-duration missions. Nonlinear rendezvous model and the possibility of handling long-duration phases were later addressed [13]. Also the asteroid rendezvous in a stochastic sense was investigated, considering the state uncertainty both of the spacecraft and the target [14] together with the optimization of correction maneuver under the Lambert's problem conditions.

Recently, general procedures of trajectory optimization under uncertainty were developed. A method transcribing the stochastic trajectory optimization into a deterministic problem by means of Polynomial Chaos Expansion and an adaptive pseudospectral collocation method was introduced by [15], while [16] presented a novel approach, based on Belief Markov Decision Process model and then applied this method to the robust optimization of a flyby trajectory of Europa Clipper mission in a scenario characterized by knowledge, execution and observation errors. Stochastic Differential Dynamic Programming has been investigated to design robust Earth–Mars transfer, considering unscented transform to propagate uncertainties [17]. This methodology has been extended subsequently using a hybrid multiple-shooting technique to overcome the limitation of the Differential Dynamic Programming [18]. More recently, the use of a combination of convex optimization and covariance steering have been introduced to solve different classes of robust continuous control problems in astrodynamics, such as interplanetary transfer [19] and reentry [20].

Lately, a full framework has been proposed to address from systematic point of view trajectory design problems, embedding uncertainties in dynamics, navigation, and control [21]. Exploiting this framework, in this work, a direct optimization approach has been developed to design robust trajectories for interplanetary small spacecraft. The robust optimal control problem is converted into a nonlinear programming problem using transcription and collocation techniques. Simultaneously, a linearized method is employed to propagate and quantify uncertainties arising from unmodeled perturbations, imperfect state knowledge, and control implementation. In order to test its performances, this methodology has been applied to the interplanetary transfer of the CubeSat M-ARGO, which is intended to be the first standalone ESA deep-space CubeSat to rendezvous with a near-Earth asteroid.

The paper is structured as follows. Section 2 introduces the robust optimization problem in a general fashion, that is specialized for the interplanetary transfer of a low-thrust small satellite in Section 3. The test case scenario is presented in Section 5. Results are shown in Section 6. Section 7 concludes the work.

2. General problem formulation

Following the optimization framework stated in [21], any robust trajectory design formulation has the aim to 1) evaluate and minimize deterministic and stochastic cost, 2) estimate the knowledge, 3) and compute the dispersion, at the same time. In order to achieve these objectives, the approach depicted in Figure 1 was devised. The initial nominal state is given together with the associated initial dispersion. For each state belonging to the initial dispersion, an initial knowledge is considered. These three quantities (nominal state, knowledge and dispersion) are propagated forward. At some prescribed times, an orbit determination process is performed in order to estimate

the true trajectory and reduce the knowledge covariance. The estimated trajectory is then used to feed the guidance scheme, compute the correction maneuver and reduce the dispersion. At the end, the final nominal state and the final dispersion can be retrieved.

It is important to stress a significant difference of this concept with respect to the traditional trajectory design. In fact, the final state is no more deterministic, but it can be more coherently represented in a stochastic way by evaluating the dispersion at the final time. Hence, it is convenient to implement the final constraint as a stochastic constraint, i.e., the final points distribution should be relatively close to the target point. Moreover, this means that the final point of the nominal trajectory will be unlikely coincident with the target.
In conclusion, the general fuel-optimal problem of a spacecraft flying in a perturbed environment under the revised approach can be formalized as:

Problem 1 (Fuel-Optimal General Problem)**.** Find the nominal state $\mathbf{x}^*(t)$, the nominal control history $\mathbf{u}^*(t)$ and, possibly, the initial and final times, t_0 and t_f, such that

$$J = \int_{t_0}^{t_f} \|\mathbf{u}^*\| \, \mathrm{d}t + Q(\Delta v^s) \tag{1}$$

with $Q(\Delta v^s)$ a measure of the stochastic cost, is minimized, while the state is subjected to a simplified Itô stochastic differential equation [22]

$$\dot{\mathbf{x}} = \mathbf{f}(\mathbf{x}, \mathbf{u}, t) + \boldsymbol{\omega}(\mathbf{x}, \mathbf{u}, t) \tag{2}$$

with $\mathbf{f}$ being the deterministic part of the dynamics and $\boldsymbol{\omega}$ the process noise associated to uncertainty in dynamics and in maneuver execution.
Moreover, the state is subjected to initial constraints

$$\begin{cases} E\left[\mathbf{x}^*(t_0)\right] = \mathbf{x}_0 \\ E\left[\left(\mathbf{x}^*(t_0) - \mathbf{x}_0\right)\left(\mathbf{x}^*(t_0) - \mathbf{x}_0\right)^T\right] = P_0^d \end{cases} \tag{3}$$

and

$$E\left[\left(\mathbf{x}(t_0) - \mathbf{x}_0\right)\left(\mathbf{x}(t_0) - \mathbf{x}_0\right)^T\right] = P_0^k \tag{4}$$

and a final constraint

$$\mathcal{E}\left(\mathbf{x}\left(t_f\right), t_f\right) \subseteq \hat{\mathcal{E}}_\delta\left(t_f\right) \tag{5}$$

with $\mathcal{E}$ indicating a generalized uncertainty ellipsoid and $\hat{\mathcal{E}}_\delta$ the desired ellipsoid.
The navigation costs are estimated through a guidance law, fed by the orbit determination scheme. It means

$$\Delta v^s = \mathtt{GL}\left(\mathbf{x}^*, \hat{\mathbf{x}}, t_{TCM}\right) \tag{6}$$

and

$$\hat{\mathbf{x}}\left(t_f^{OD}\right) = \mathtt{OD}\left(\mathbf{x}, \hat{\mathbf{x}}, t_0^{OD}, t_f^{OD}\right) \tag{7}$$

with GL and OD being the Guidance Law and orbit determination procedures respectively, $\hat{\mathbf{x}}$ is the estimated state, $\mathbf{x}$ the real state and $\mathbf{x}^*$ is the nominal state.

Within this approach, three main building blocks can be identified and they are: 1) a procedure to quantify uncertainty and to evaluate the stochastic measures, 2) a knowledge analysis method with an OD scheme, and 3) a dispersion analysis method with a guidance law, that can vary and should be selected properly.

3. Methodology

Problem 1 must be adapted to the interplanetary transfer of a small satellite equipped with low-thrust continuous propulsion. Knowledge and dispersion analyses are performed exploiting two different techniques in order to cope with the characteristics of a spacecraft having a continuous thrust, that should be modeled as a stochastic process. For this reason:

- *Knowledge analysis* is performed employing local linearization in a fashion similar to [23];
- *Dispersion analysis* is achieved by using a Monte Carlo simulation.

3.1 State and uncertainty propagation

A spacecraft in deep space is considered to by subjected to the gravitational attraction of the Sun and the planets, with the additional effect of the SRP. Considering spherical coordinates, the states are defined as $\mathbf{x} = [r, \theta, \phi, v_r, v_\theta, v_\phi, m]$, with ϕ and θ the Azimuth and Elevation angles in J2000 respectively, while the control vector is $\mathbf{u} = [T, \alpha, \beta]$, with α taken from $\hat{\theta}$-vector in the orbit plane, while β is the out-of-plane thrust angle. In this case, the spacecraft dynamics can be written as

$$\dot{\mathbf{x}} = \mathbf{f}(\mathbf{x}, \mathbf{u}, t) = \begin{bmatrix} v_r \\ \frac{v_\theta}{r\cos\phi} \\ \frac{v_\phi}{r} \\ P\left(\mathbf{f}_G + \mathbf{f}_{SRP}\right) + S\begin{bmatrix} v_r \\ v_\theta \\ v_\phi \end{bmatrix} + \mathbf{f}_T \\ -\frac{T}{I_{sp} g_0} \end{bmatrix} \tag{8}$$

The gravitational force is

$$\mathbf{f}_G = -\frac{\mu}{r^3}\mathbf{r} - \sum_{i \in \mathcal{P}} \mu_i \left(\frac{\mathbf{r}_i}{r_i^3} - \frac{\mathbf{r}_i - \mathbf{r}}{\|\mathbf{r}_i - \mathbf{r}\|^3} \right) \tag{9}$$

where $\mathbf{r}$ is the position vector of the spacecraft in J2000 and r is its magnitude, $\mathbf{r}_i$ is the i-th planet position vector and r_i its magnitude, and μ_i is the planetary gravitational constant. The symbol $\mathcal{P}$ indicates a set containing all the

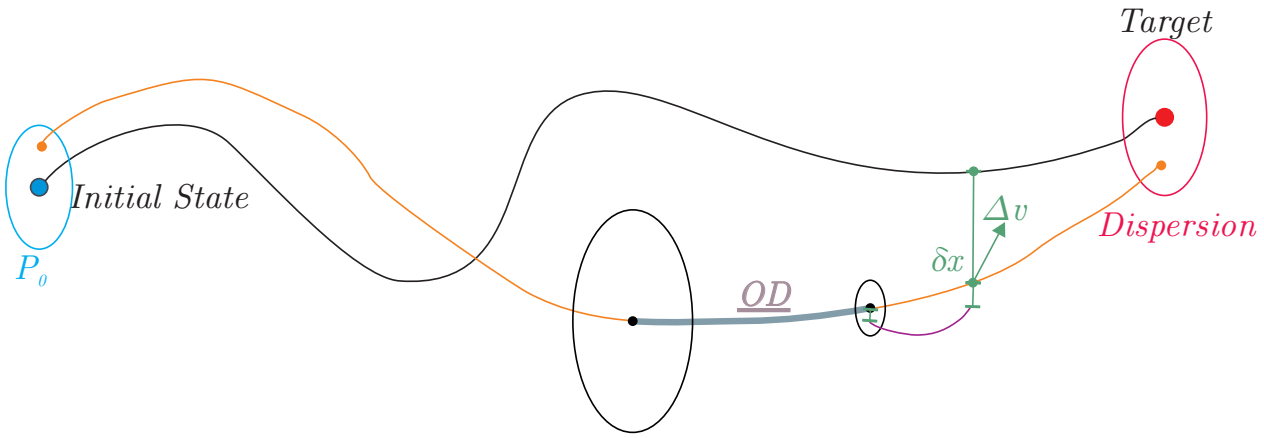

Fig. 1. Revised approach for the preliminary mission analysis. Nominal trajectory is indicated with a black line, a true possible trajectory with an orange line, estimated trajectory with a magenta line. The OD process is the gray thick line. Black ellipses represent the instantaneous knowledge; colored ellipses represent the dispersion.

planet of the Solar System. Planet states are retrieved by means of SPICE kernels [24]. The SRP is defined as

$$\mathbf{f}_{SRP} = \frac{QA}{m}\frac{\mathbf{r}}{r^3} \tag{10}$$

where Q is the solar pressure constant.
The thrust vector is written as

$$\mathbf{f}_T = \frac{T}{m}\begin{bmatrix}\sin\alpha\cos\beta\\ \cos\alpha\cos\beta\\ \sin\beta\end{bmatrix} \tag{11}$$

while the matrices P and S are

$$P = \begin{bmatrix}\cos\phi\cos\theta & \cos\phi\sin\theta & \sin\phi\\ -\sin\theta & \cos\theta & 0\\ -\sin\phi\cos\theta & -\sin\phi\sin\theta & \cos\phi\end{bmatrix}$$

$$S = \begin{bmatrix}0 & \dot\theta\cos\phi & \dot\phi\\ -\dot\theta\cos\phi & 0 & \dot\theta\sin\phi\\ -\dot\phi & -\dot\theta\sin\phi & 0\end{bmatrix}$$

On the other hand, due to the limited nonlinearity effects associated to low-thrust interplanetary trajectories, uncertainties can be propagated by means of a linearized approach [23].
Dynamics and control error are modeled as Gauss–Markov process, also know as exponential-correlated random variables. A Gauss–Markov process obeys Langevin differential equation [23], i.e.,

$$\dot\omega(t) = -\beta\omega(t) + u(t) \tag{12}$$

where ω is the Gauss–Markov process, u is a white noise with a given variance, and $\beta = 1/\tau$ is the inverse of the correlation time.
Defining the deviation of the real state from the nominal one as

$$\delta\mathbf{x}(t) = \mathbf{x}(t) - \mathbf{x}^*(t) \tag{13}$$

while the *process noise* vector as $\boldsymbol{\omega}(t) \in \mathbb{R}^{3d}$, where d is the number of stochastic processes, the extended state, including both the state and the process noise, is

$$\boldsymbol{\chi}(t) = \begin{bmatrix}\delta\mathbf{x}(t)\\ \boldsymbol{\omega}(t)\end{bmatrix} \tag{14}$$

An associated state transition matrix (STM) can be stated as

$$\tilde\Phi(t_0,t) = \frac{\partial\boldsymbol{\chi}(t)}{\partial\boldsymbol{\chi}(t_0)} = \begin{bmatrix}\Phi & M\\ 0_{3d\times n} & W\end{bmatrix} \tag{15}$$

where n is the number of the states. The matrix Φ is the STM associated to the free dynamics in Eq. (8), that satisfy the variational equation

$$\dot\Phi = A\Phi \tag{16}$$

with $A = \partial\mathbf{f}/\partial\mathbf{x}$, while matrices M and W represent the derivative of the process noise with respect to the state deviation and itself, respectively. Recalling that process noises satisfy Eq. (12), for a given process [23]

$$M_i = \frac{\partial\mathbf{x}(t)}{\partial\boldsymbol{\omega}_i(t_0)} = \begin{bmatrix}\left[\frac{1}{\beta}\delta t + \frac{1}{\beta^2}\left(e^{-\beta\delta t}-1\right)\right]I_3\\ \frac{1}{\beta}\left(1-e^{-\beta\delta t}\right)I_3\\ \mathbf{0}_3\end{bmatrix} \tag{17}$$

where M_i represents the block of matrix M associated to the i-th 3-dimensional process noise $\boldsymbol{\omega}_i$ and $\delta t = t - t_0$, while

$$W_i = \frac{\partial\boldsymbol{\omega}_i(t)}{\partial\boldsymbol{\omega}_i(t_0)} = \left[e^{-\beta\delta t}I_3\right] \tag{18}$$

The extended state can be propagated forward by using the

extended STM, thus

$$\boldsymbol{\chi} = \tilde{\Phi}\left(t_0, t\right)\boldsymbol{\chi}_0 + \Gamma\left(t_0, t\right)\boldsymbol{u}_0 \tag{19}$$

the $\boldsymbol{u}_0$ is the realization of a standard white noise and

$$\Gamma\left(t_0, t\right) = \int_{t_0}^{t} \tilde{\Phi}\left(t_0, \tau\right) B(\tau)\, \mathrm{d}\tau \tag{20}$$

is the process noise transition matrix and the $B = [0_n,\, I_{3d}]^T$.
Consequently, the state covariance matrix can be propagated with

$$P = \tilde{\Phi}\left(t, t_0\right) P_0 \tilde{\Phi}^T\left(t_0, t\right) + \int_{t_0}^{t} \tilde{\Phi}\left(t_0, \tau\right) B(\tau) Q(\tau) B^T(\tau) \tilde{\Phi}^T\left(t_0, \tau\right)\, \mathrm{d}\tau \tag{21}$$

with $Q(\tau)$ is the covariance matrix of the process noises.

3.2 Knowledge analysis method

The spacecraft state knowledge during the interplanetary transfer is improved by an OD algorithm, exploiting radiometric measures coming from on-ground facilities. Radiometric data for range and range-rate are simulated, generating pseudo-measurements as

$$\gamma = \sqrt{\boldsymbol{\gamma}^T\boldsymbol{\gamma}}, \qquad \dot{\gamma} = \frac{\boldsymbol{\gamma}^T\boldsymbol{\eta}}{\gamma} \tag{22}$$

where γ is the range, $\dot{\gamma}$ is the range rate, $\boldsymbol{\gamma} = \mathbf{r} - \mathbf{r}_{GS}$ is the relative distance between the spacecraft and the ground station, while $\boldsymbol{\eta} = \mathbf{v} - \mathbf{v}_{GS}$ is the relative velocity. Pseudo-measurements can be performed only if a link between the spacecraft and the selected ground station can be established, i.e., only when some geometric conditions are verified, that are

- the Sun exclusion angle ϕ should be greater than a prescribed value in order to avoid degradation in the radiometric observable and, in turn, in the trajectory knowledge [25];
- the spacecraft elevation above the ground El in ground station location should be higher than a minimum value El_{min} in order to avoid low-quality data related to the atmospheric extinction of the radiometric signal and to cope with the mounting constraints of the ground station sensor.

Pseudo-measurements are then used to feed an extended Kalman filter (EKF) [23] in order to estimate the spacecraft state.

3.3 Dispersion analysis method

The stochastic Δv is estimated by exploiting a Monte Carlo simulation on the linearized trajectory. The correction maneuvers are computed by exploiting the differential guidance (DG)

$$\begin{aligned}\Delta\mathbf{v}_k^s = &-\left(\Phi_{rv}^T\Phi_{rv} + q\Phi_{vv}^T\Phi_{vv}\right)^{-1} \\ &\left(\Phi_{rv}^T\Phi_{rr} + q\Phi_{vv}^T\Phi_{vr}\right)\widetilde{\delta\mathbf{r}}_k - \widetilde{\delta\mathbf{v}}_k\end{aligned} \tag{23}$$

with

$$\widetilde{\delta\mathbf{x}}_k = \delta\mathbf{x}_k + \mathcal{N}\left(\bar{\mathbf{X}}_k, P_k\right) \tag{24}$$

with $\mathbf{X}_k$ and P_k output of the EKF filter.
For each sample, the Δv_k^s are converted in needed propellant mass by the Tsiolkovsky equation

$$m_p^s(t_k) = m_k\left(1 - e^{-\frac{\Delta v^s}{g_0 I_{sp}^c}}\right) \tag{25}$$

Even if the spacecraft mass should be reduced by the stochastic correction, this behavior is not considered, since its effects are limited.
Once the stochastic propellant mass is computed for each Monte Carlo sample, the kernel quantile estimation (KQE) is used for the quantile evaluation. The quantile function is the left-continuous inverse of the cumulative distribution function

$$Q(p) = \inf\{q : F(q) \le p\} \qquad \text{with} \quad 0 \le p \le 1 \tag{26}$$

i.e., the function returning the threshold value of q, such that the probability variable being less than or equal to that value equals the given probability p. Using the LQE, the quantile function can be computed as [26]

$$Q(p, q) = \sum_{j=1}^{n} \frac{1}{nh} K\left[\frac{1}{h}\left(\frac{j}{n} - p\right)\right]\tilde{q}_j \tag{27}$$

where $\tilde{q}_j,\ j = \{1, \ldots n\}$ is the sorted set of q_j and K is the kernel function. The use of this linear KQE formula give the possibility to obtain reliable estimation for the desired quantile value, while having a $\mathcal{C}^\infty$-class function. Indeed, although Monte Carlo is used to compute the navigation costs, and, thus a simple samples counting is possible, the use of KQE gives smooth, continuous derivatives and, for this reason, it is preferred.
As per the framework in this work, the final dispersion can be evaluated by exploiting Monte Carlo final states. Indeed, it is possible to retrieve mean $\bar{\mathbf{X}}$ and covariance P for the error with respect to the nominal final state. These value can be used to build an uncertainty ellipsoid [23], useful to infer information on the state uncertainty at a given time. Since P is a positive-definite real matrix, it is always possible to diagonalize it by applying the spectral theorem. Thus

$$D = \begin{bmatrix}\lambda_1 & 0 & 0 \\ 0 & \lambda_2 & 0 \\ 0 & 0 & \lambda_3\end{bmatrix} = U^T P U \tag{28}$$

with λ_i are the eigenvalues and $U = [\mathbf{u}_1, \mathbf{u}_2, \mathbf{u}_3]$ is an orthonormal matrix, containing the eigenvectors as columns. The principal axes of P are

$$\hat{\mathbf{r}}' = \begin{bmatrix} \hat{x}' \\ \hat{y}' \\ \hat{z}' \end{bmatrix} = U^T \hat{\mathbf{r}} \tag{29}$$

where $\hat{\mathbf{x}}$ are the J2000 axes. Eventually, the probability ellipsoid is defined as

$$\frac{\hat{x}'^2}{\lambda_1} + \frac{\hat{y}'^2}{\lambda_2} + \frac{\hat{z}'^2}{\lambda_3} = \sigma^2 \tag{30}$$

where σ is the confidence level desired expressed in standard deviation levels. Thus, the uncertainty ellipsoid will be defined as the ellipsoid having as semi-major axes $\sqrt{\lambda_i}$, oriented as the direction of the eigenspace principal axes associated to the covariance matrix.

At the final time, it is desirable that the trajectory ellipsoid is contained at a certain confidence level inside the asteroid uncertainty ellipsoid, i.e.,

$$\mathcal{E}\left(\mathbf{x}\left(t_f\right), t_f\right) \subseteq \mathcal{E}_{Ast}\left(t_f\right) \tag{31}$$

This condition can be checked by performing an eigenvalue analysis on the ellipsoid representing matrices [33]. Generally speaking, a 3D ellipsoid can be represented using a matrix formulation

$$ZTCT^T Z^T = 0 \tag{32}$$

with $Z = [x, y, z, 1]^T$, where

$$C = \begin{bmatrix} P^{-1} & \mathbf{0}_3 \\ \mathbf{0}_3^T & -1 \end{bmatrix} \tag{33}$$

is a matrix containing dimensions and axis direction of the ellipsoid, and

$$T = \begin{bmatrix} I & \mathbf{0}_3 \\ -\mathbf{x}_f & 1 \end{bmatrix} \tag{34}$$

is the translation matrix, used to bring the center of the ellipsoid in $\mathbf{x}_f$ (i.e., $\mathbf{x}^*(t_f) + \bar{\mathbf{X}}$ for the spacecraft and $\mathbf{x}_{Ast}(t_f)$ for the target). Defining A the matrix TCT^T for the spacecraft and B the one of the asteroid, it is possible to show that the condition in Eq. (31) is mathematically equivalent to [33]

$$\begin{cases} \text{Im}\left(\text{eig}\left(A^{-1}B\right)\right) = 0 \\ \text{eig}\left(A^{-1}B\right) \geq 1 \end{cases} \tag{35}$$

Thus, the eigenvalues of matrix $A^{-1}B$ should be real and grater than the unity.

4. Problem formulation

Once the methodology has been defined, the general optimal control problem should be translated in a nonlinear programming problem (NLP) so that it can be solved numerically.

Usually, interplanetary transfers are made by only few revolutions about the Sun. Thus, tackling this problem should not require an excessive amount of parameters to represent the time-variation of state and controls, if a direct problem is exploited. Moreover, the high-fidelity equations of motion becomes computational intensive, reducing the effectiveness of indirect or shooting approaches. Therefore, a direct method using collocation is judged to have the best balance between computational time and accuracy.

In this case, the time is discretized evenly in N nodes $t_d = t_0 < t_1 < \cdots < t_N = t_f$ and states are enforced over this grid, with the control approximated linearly. So, for each time t_k, the following quantities can be defined

$$\mathbf{x}(t_k) = \mathbf{x}_k, \qquad \mathbf{u}(t_k) = \mathbf{u}_k, \qquad \forall\ k = 0, \ldots, N \tag{36}$$

while in each segment

$$t_k \leq t \leq t_{k+1}, \qquad \mathbf{u}(t) = \mathbf{u}_k + \frac{t - t_k}{t_{k+1} - t_k}\left(\mathbf{u}_{k+1} - \mathbf{u}_k\right) \tag{37}$$

For each segment continuity of the solutions at both ends is enforced. The defect constraints ζ_k are constructed by using an Hermite-Simpson quadrature scheme

$$\zeta_k = \mathbf{x}_{k+1} - \frac{h}{6}\left(\mathbf{f}_k + 4\mathbf{f}_c + \mathbf{f}_{k+1}\right) \tag{38}$$

with

$$\mathbf{f}_k = \mathbf{f}(\mathbf{x}_k, \mathbf{u}_k, t_k), \qquad \mathbf{f}_{k+1} = \mathbf{f}(\mathbf{x}_{k+1}, \mathbf{u}_{k+1}, t_{k+1})$$

$$\mathbf{f}_c = \mathbf{f}(\mathbf{x}_c, \mathbf{u}_c, t_c)$$

and the central points are defined as

$$t_c = t_k + \frac{h}{2}, \qquad \mathbf{x}_c = \frac{1}{2}\left(\mathbf{x}_k + \mathbf{x}_{k+1}\right) + \frac{h}{8}\left(\mathbf{f}_k - \mathbf{f}_{k+1}\right)$$

$$\mathbf{u}_c = \frac{1}{2}\left(\mathbf{u}_k + \mathbf{u}_{k+1}\right)$$

with the time step being $h = t_{k+1} - t_k$, constant by construction.

Thus, the robust optimization problem for an interplanetary transfer of a low-thrust spacecraft can be stated as

Problem 2 (Fuel-optimal robust optimization problem)**.** Find the variable vector

$$\mathbf{y} = [\mathbf{x}_1^*,\ \ldots,\ \mathbf{x}_N^*,\ \mathbf{u}_1,\ \ldots,\ \mathbf{u}_N] \tag{39}$$

minimizing the cost function

$$J(\mathbf{y}) = -\left(m(t_f) - Q\left(0.99, m_s\right)\right) \tag{40}$$

i.e., maximizing the sum of the mass at the final time and a measure of the propellant mass needed for the stochastic correction (Eq. (25)) computed through the KQE, subjected to the equality constraints:

- Defect vectors for the nominal state must be null to ensure continuity between adjoint segments:

$$\zeta_k = 0, \qquad \forall\ k \in \{1,\ N\} \tag{41}$$

- Boundary condition at the initial time is enforced:

$$\begin{cases} E\left[\mathbf{x}^*(t_0)\right] = \mathbf{x}_0 = \mathbf{x}(t_0) \\ E\left[\left(\mathbf{x}^*(t_0) - \mathbf{x}_0\right)\left(\mathbf{x}^*(t_0) - \mathbf{x}_0\right)^T\right] = P_0 \\ m(t_0) = m_0 \end{cases} \tag{42}$$

- Stochastic boundary condition on the final state must be satisfied:

$$\begin{cases} \text{Im}\left(\text{eig}\left(A^{-1}B\right)\right) = 0 \\ \text{eig}\left(A^{-1}B\right) \geq 1 \end{cases} \tag{43}$$

and to the inequality constraints:

- Thrust cannot overcome its allowable maximum value:

$$T - T_{\text{max}} \leq 0 \tag{44}$$

- Final mass must be positive:

$$-m(t_f) \leq 0 \tag{45}$$

The procedure used to estimate relevant quantities for the optimization problem are collected in Algorithm 1.

5. Test case scenario

In order to evaluate performances of Problem 2, a test case scenario is identifies and it is the interplanetary transfer of the CubeSat M-ARGO.

5.1 The CubeSat M-ARGO

The Miniaturised Asteroid Remote Geophysical Observer (M-ARGO) is planned to be the first standalone ESA deep-space CubeSat to rendezvous a near-Earth asteroid (NEA) [27]. The M-ARGO concept was developed by ESA's Concurrent Design Facility. In 2019, ESA funded the Phase A study, that was conducted by GomSpace Luxemburg in collaboration with Politecnico di Milano. M-ARGO successfully passed the MDR in November 2019 and the PRR in July 2020.

The M-ARGO project foresaw a 12U CubeSat, planned to piggyback on the launch of another large spacecraft going towards the Sun–Earth Lagrange point L_2. After insertion into a parking orbit at L_2, M-ARGO will perform a deep-space cruise towards a NEA target using low-thrust electric propulsion, demonstrating the capability of CubeSats to independently explore deep-space objects.
In the scenario presented in Phase A, M-ARGO is departing from the Sun–Earth L_2 point between January 01, 2023 and December 31, 2024 and shall reach a selected target in less than 3 years, with available propellant amounting to $m_{p,\text{max}} = 2.8\,\text{kg}$. Characteristics of the spacecraft and the transfer are given in Table 1.

5.1.1 Thruster model

In order to simulate accurately the available thrust and instantaneous specific impulse, a realistic model for the M-ARGO thruster is implemented. This feature is important in case of limited-capability low-thrust spacecraft since it helps in precisely define the CubeSat maneuver capability. The thruster model assumes that both the maximum thrust, T_{max}, and the specific impulse, I_{sp}, depend on the instantaneous input power, P_{in}, which in turn is a function of the Sun distance, r. It means that

$$T_{\text{max}} = T_{\text{max}}(P_{in}), \quad I_{sp} = I_{sp}(P_{in}), \quad P_{in} = P_{in}(r) \tag{46}$$

In order to correctly represent functions in Eq. (46), fourth-order polynomials are employed. They are able to correctly represent the behavior of the M-ARGO electric power system and miniaturized ion thruster, while having smooth, non-singular derivatives. Thus

$$T_{\text{max}}(P_{in}) = a_0 + a_1 P_{in} + a_2 P_{in}^2 + a_3 P_{in}^3 + a_4 P_{in}^4 \tag{47}$$

$$I_{sp}(P_{in}) = b_0 + b_1 P_{in} + b_2 P_{in}^2 + b_3 P_{in}^3 + b_4 P_{in}^4 \tag{48}$$

$$P_{in}(r) = c_0 + c_1 r + c_2 r^2 + c_3 r^3 + c_4 r^4 \tag{49}$$

Moreover, the thruster input power is characterized by upper and lower boundaries, $P_{in,\text{min}}$ and $P_{in,\text{max}}$, respectively, due to technological constraints, related to the managing of thermal and power subsystems. For this reason, a saturation logic is considered and it is

$$\begin{aligned} \text{if } P_{in}(r) > P_{in,\text{max}} \quad &\text{then} \quad P_{in} = P_{in,\text{max}},\ T_{\text{max}} = T_{\text{max}}(P_{in}),\ I_{sp} = I_{sp}(P_{in}) \\ \text{if } P_{in} \in [P_{in,\text{min}}, P_{in,\text{max}}] \quad &\text{then} \quad P_{in} = P_{in}(r),\ T_{\text{max}} = T_{\text{max}}(P_{in}),\ I_{sp} = I_{sp}(P_{in}) \\ \text{if } P_{in}(r) < P_{in,\text{min}} \quad &\text{then} \quad P_{in} = P_{in}(r),\ T_{\text{max}} = 0,\ I_{sp} \text{ not defined} \end{aligned}$$

The coefficients and the input power limits used in the mission analysis are given in Table 2. A graphical representation of the thruster model is reported in Figure 2. Parameters at 1 AU can be retrieved from those data, and they are

- Input power of 105.4 W;
- Maximum thrust of 1.89 mN and thrust-to-mass ratio

Algorithm 1: Fuel-optimal robust optimization problem algorithm

Procedure INTEGRATED APPROACH
- Define spacecraft and navigation settings, and uncertainty properties;
- **Function** INITIALIZATION
  - Compute the random variables for the Monte Carlo simulation;
- **Function** KNOWLEDGE ANALYSIS
  - Consider the nominal trajectory;
  - **for** $i = 1$ **to** n_P ▷Loop through n_P sub-phases
    - **switch** *sub-phase*
      - **case** *OD phase*
        - **Function** ORBIT DETERMINATION
          - Find the visibility windows;
          - Retrieve the n_M measurement times t_k;
          - **for** $k = 1$ **to** n_M ▷Loop through n_M meas. times
            - Retrieve observation data;
            - Generate the pseudo-measurement;
            - Apply the EKF;
            - Get mean and covariance from the filter;
            - Propagate mean and coviariance to t_{k+1};
          - **end**
          - Propagate mean and coviariance up to the final time t_f^{OD};
        - **Result:** $\bar{X}_k$ and P_k at each OD final time
      - **otherwise**
        - Propagate statistics up to the *final sub-phase* time;
    - **end**
  - **end**
- **Result:** Knowledge time evolution
- **Function** NAVIGATION COSTS & FINAL ELLIPSOID
  - **for** $\forall$ *Monte Carlo sample*
    - **for** $i = 1$ **to** n_P ▷Loop through n_P sub-phases
      - **switch** *sub-phase*
        - **case** *Thrusting phase*
          - Propagate the deviation up to the TCM time;
          - Estimate the correction maneuvers; ▷See Eq. (23)
          - Compute the needed propellant mass; ▷See Eq. (25)
          - Apply the maneuvers to each sample;
        - **case** *OD phase*
          - Propagate the the deviation up to the final OD time;
          - Evaluate the estimated deviaton; ▷See Eq. (24)
      - **end**
    - **end**
  - **end**
  - Compute the final state ellipsoid;
- **Result:** Navigation cost estimate; Final state ellipsoid

Result: Cost function (Eq. (40)); Dispersion statistic (Eq. (43))

Table 1. M-ARGO mission time-frame and spacecraft data.

Departure window	**Transfer**	m_0	$m_{p,\max}$	A/m	c_r
2023 – 2024	≤ 3 years	22.6 kg	2.8 kg	0.013 27 m^2/kg	1.3

of 8.36×10^{-5} m/s^2;

- Specific impulse of 3022.59 s.

Moreover, trajectory correction maneuvers are performed using the same thruster, but in a cold gas fashion. This feature is a characteristic of the M-ARGO propulsive system. In this case, $I_{sp}^{c} = 40$ s.

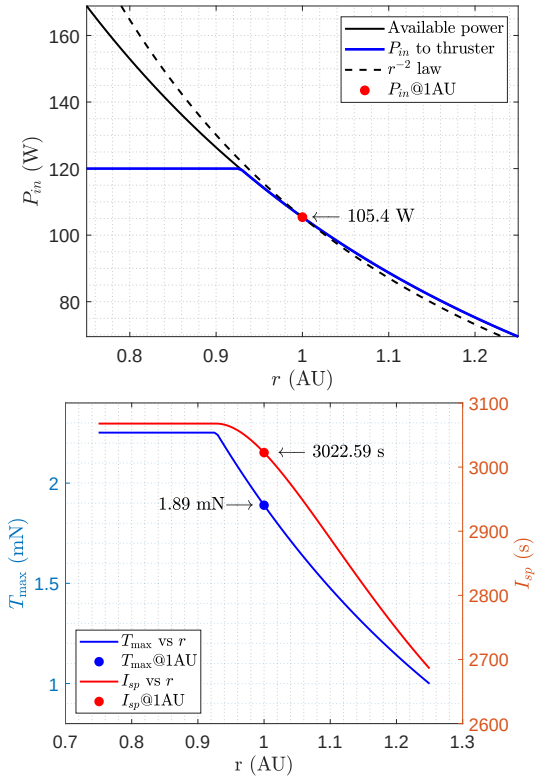

Fig. 2. Graphical representation of the M-ARGO thruster model.

5.2 ConOps

In order to solve Problem 2 and apply Algorithm 1, the concept of operations (ConOps) for M-ARGO must be defined. In order to have a regular and repetitive operations pattern, M-ARGO trajectory from L_2 to the target asteroid is subdivided into two legs, repeating cyclically, as shown in Figure 3:

1. From day 0 to day 6 of each week: *thrusting phase*;
2. From day 6 to day 7 of each week: *OD phase*.

During the OD phase, on-ground teams will perform orbit determination processes, compute trajectory correction maneuvers to compensate for the state deviations and send proper commands to the spacecraft. In a real life scenario, the spacecraft will shut down the thruster during the OD phase, since a large amount of power is required to communicate with the Earth and angles are locked in order to point the antenna toward the ground. However, in this test case, operation compliance is not considered in order to simplify the dynamics and the optimization.

Fig. 3. M-ARGO transfer ConOps. The grey bars represents the OD phases, while the green arrows mark the TCMs points. Time in days after the departure time from L_2.

5.3 First guess generation

In order to test M-ARGO, a nominal trajectory, serving also as the deterministic benchmark should be selected. The target selection work in [29] is exploited to find a first guess. Among $700,000$ asteroids analyzed, 5 were shortlisted, based on feasibility, future observability, transfers properties, asteroid characteristics, and costs, and they are

1. **2014 YD**: Known high spin rate; favorable mission opportunity;
2. **2010 UE51**: #1 on time-optimal and fuel-optimal solution list;
3. **2011 MD**: Present in light curve database, favorable mission opportunity;
4. **2000 SG344**: Observable in the near future, inclined, low uncertainty;
5. **2012 UV136**: Known spin rate, largest target size

For each shortlisted asteroid, a baseline and backup trajectory are selected, following these criteria:

1. Sensitivity of m_p both in horizontal (Dep. Date) and vertical (ToF) direction;
2. Far from the boundaries in order to surely have feasible solutions;
3. Baseline solution is chosen between 01 Jan 2023 and 31 Dec 2023, in order to have a backup in the year 2024;
4. Among solutions with the same m_p, a lower Time of Flight is preferred.

Table 2. Thruster model parameters (r in Eq. (49) is in AU).

Version	$T_{\max}$ coeff. (mN)	I_{sp} coeff. (s)	P_{in} coeff. (W)
	$a_0 = -0.7253$	$b_0 = 2652$	$c_0 = 840.11$
	$a_1 = 0.02481$	$b_1 = -18.123$	$c_1 = -1754.3$
v 1.0 (07/07/2019)	$a_1 = 0.02481$	$b_1 = -18.123$	$c_1 = -1754.3$
	$a_1 = 0.02481$	$b_1 = -18.123$	$c_1 = -1754.3$
$P_{in,\min} = 20\,\mathrm{W}$	$a_2 = 0$	$b_2 = 0.3887$	$c_2 = 1625.01$
$P_{in,\max} = 120\,\mathrm{W}$	$a_3 = 0$	$b_3 = -0.00174$	$c_3 = -739.87$
	$a_4 = 0$	$b_4 = 0$	$c_4 = 134.45$

Without loss of generality, the baseline trajectory of asteroid 2000 SG344, having the characteristics in Table 4, is used as test case scenario in this work. Keplerian parameters for the target asteroid are given in Table 3. Asteroid 2000 SG344 is chosen as nominal target due to the repeatability of its porkchop pattern and the needed low propellant.

6. Results

In order to solve Problem 2, the tool DIRETTO internally developed at Politecnico di Milano [30] is exploited for this task. The software IpOpt [32], in the implementation by OPTI Toolbox*, is exploited to solve the optimization problem, by means of an internal point method.
States for both L_2 and Asteroid are retrieved using SPICE kernels, while target covariance at the final time is retrieved by exploiting a telnet connection with NASA Horizon system [34]. Asteroid covariance matrix is retrieved at some specific times and then interpolated by means of a cubic splines using not-a-knot end conditions, in order to have a $\mathcal{C}^2$-class function.
A standard deviation σ of 1000 km in position and 1 m/s in velocity are used for all the Cartesian components of the uncertain initial state. No uncertainty is considered for the spacecraft mass. The random processes considered in the simulations are listed in Table 5.
Additionally, the ground station considered is the 35-meter DSA-1 antenna by ESTRACK, located in New Norcia, Australia. Its performances are in Table 6.
Optimization results are reported in Table 7 together with results associated to the first guess. Exploiting a good educated guess, the optimization algorithm requires only 5 minutes on a quad-core Intel i7@2.80GHz to converge.
The optimization under the revised approach leads to savings in propellant mass amounting to 3%. However, if only the stochastic component is considered, the needed propellant mass in the optimized case is only a half with respect to the first guess one. This result is obtained by flying a trajectory with lower dispersion. In the optimized case, the spacecraft thrusts during the last powered arc in a region with a lower maximum thrust. Since the dispersion depends on the thrust magnitude, a lower thrust level means lower dispersion and, thus, TCMs. Additionally, knowledge analysis is shown in Figure 5. Final state uncertainty ellipsoids are depicted in Figure 6. The asteroid position uncertainty, taken from the HORIZON system, is an order of magnitude higher than the 3σ trajectory ellipsoid, deeming feasible the transfer to a wide extent.

*See `https://github.com/jonathancurrie/OPTI` (Last retrieved on September 13, 2024.)

7. Conclusions

In this work, a robust trajectory optimization approach has been developed for interplanetary transfers and successfully applied to the CubeSat M-ARGO. By incorporating uncertainties directly in the optimization, the method addresses the limitations of traditional trajectory design, which rely on nominal trajectory optimization followed by an analysis correction maneuvers. The proposed methodology leverages on a direct collocation method embedding linear uncertainty quantification, leading to significant reductions in propellant mass and trajectory correction maneuvers. The results demonstrate that, compared to the traditional full-deterministic design, the stochastic approach yields a 50% reduction in the navigation cost, highlighting the benefits of accounting for uncertainties in early trajectory design. This method enables CubeSats with limited propulsion capabilities to achieve deep-space missions with enhanced robustness and efficiency.

References

[1] W. Fehse, *Automated rendezvous and docking of spacecraft*. Cambridge University Press, 2003, vol. 16.

[2] A. Poghosyan and A. Golkar, "CubeSat evolution: Analyzing CubeSat capabilities for conducting science missions," *Progress in Aerospace Sciences*,

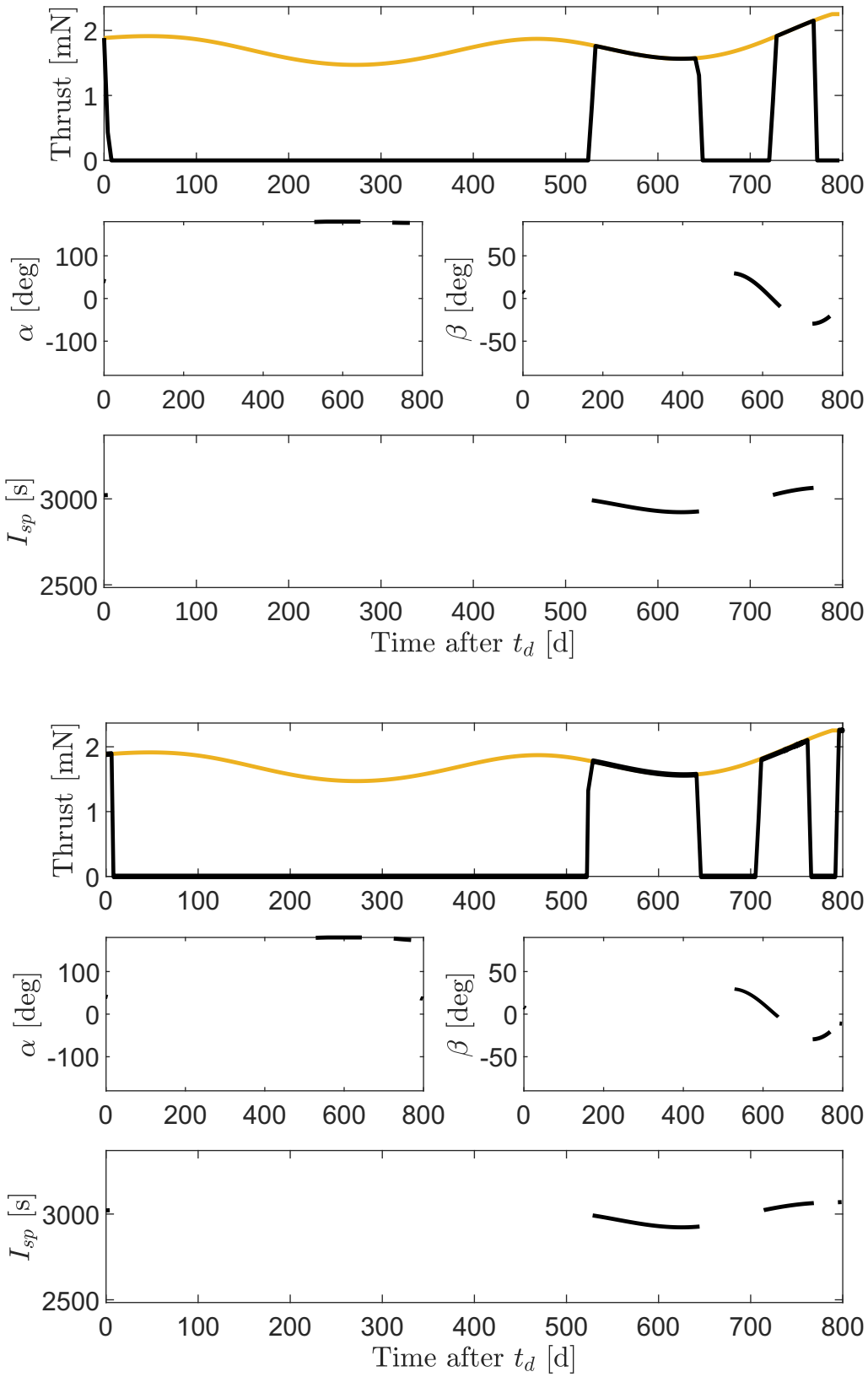

Fig. 4. Control profile for M-ARGO baseline solution to 2000 SG344: (a) First guess; (b) Optimized.

Table 3. Orbital elements for the asteroid 2000 SG344.

Name	a [AU]	e [-]	i [deg]	ω [deg]	Ω [deg]
2000 SG344	0.9775	0.0669	0.1121	275.3026	191.9599

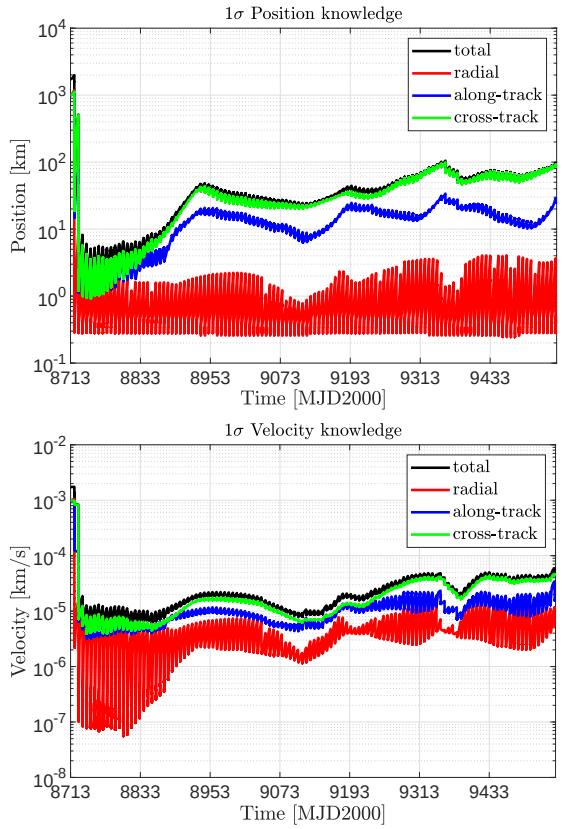

Fig. 5. Knowledge analysis for 2000 SG344 Baseline Optimized Trajectory: (a) Position; (b) Velocity.

Table 4. Characteristics of baseline solution for M-ARGO.

Name	**Departure Date**	**TOF [d]**	m_p [kg]
2000 SG344	09 NOV 2023	796	0.857

Table 5. M-ARGO Gauss–Markov processes.

Uncertain process	σ	τ
Solar radiation pressure	10% in magnitude	1 d
Thrust	1% in magnitude	1 d
	1° in pointing angles	1 d
Residual acceleration	1×10^{-11} km/s^2	1 d

Table 6. Assumed characteristics for New Norcia ground station.

Parameter	**Value**
Coordinates	31.048 225° S 116.1915° E
Altitude	0.2523 km
Range meas. frequency	twice per pass
Doppler meas. frequency	once every 10 min
Range meas. random error (1σ)	200 m
Range meas. systematic error	200 m
Doppler meas. random error (1σ)	0.3 mm/s
Doppler meas. systematic error	0 mm/s
Station coordinates in plane (1σ)	30 cm
Station coordinates out of plane (1σ)	1 m
Minimum elevation El_{min}	15°

vol. 88, pp. 59–83, 2017. DOI: 10.1016/j.paerosci.2016.11.002.

[3] R. Walker *et al.*, "Deep-space CubeSats: Thinking inside the box," *Astronomy & Geophysics*, vol. 59, no. 5, pp. 24–30, 2018. DOI: 10.1093/astrogeo/aty232.

[4] R. S. Park and D. J. Scheeres, "Nonlinear mapping of Gaussian statistics: Theory and applications to spacecraft trajectory design," *Journal of Guidance, Control, and Dynamics*, vol. 29, no. 6, pp. 1367–1375, 2006. DOI: 10.2514/1.20177.

Table 7. Revised approach solution for M-ARGO case.

	ToF [d]	m_p (det.) [kg]	m_p (stoc.) [kg]	m_p **(Total)** [kg]
First Guess	796	0.857	0.067	0.924
Optimized	798.12	0.858	0.038	0.896

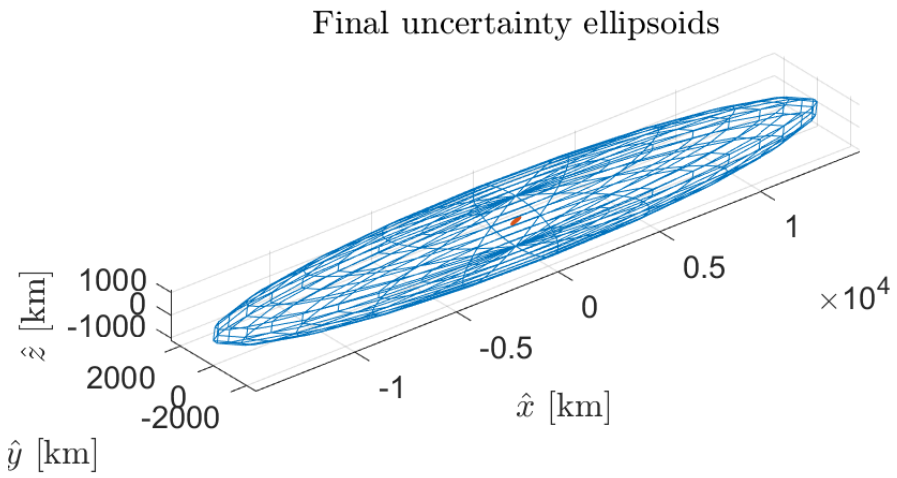

Fig. 6. Final time uncertainty ellipsoids for the optimized M-ARGO case. Asteroid ellipsoid is shown in blue, while the spacecraft 3σ ellipsoid is depicted in red.

[5] P. Di Lizia, R. Armellin, A. Ercoli-Finzi, and M. Berz, "High-order robust guidance of interplanetary trajectories based on differential algebra," *Journal of Aerospace Engineering, Sciences and Applications*, vol. 1, no. 1, pp. 43–57, 2008.

[6] P. Di Lizia, R. Armellin, F. Bernelli-Zazzera, and M. Berz, "High order optimal control of space trajectories with uncertain boundary conditions," *Acta Astronautica*, vol. 93, pp. 217–229, 2014. DOI: 10.1016/j.actaastro.2013.07.007.

[7] P. Di Lizia, R. Armellin, A. Morselli, and F. Bernelli-Zazzera, "High order optimal feedback control of space trajectories with bounded control," *Acta Astronautica*, vol. 94, no. 1, pp. 383–394, 2014. DOI: 10.1016/j.actaastro.2013.02.011.

[8] P. W. Schumacher Jr, C. Sabol, C. C. Higginson, and K. T. Alfriend, "Uncertain Lambert Problem," *Journal of Guidance, Control, and Dynamics*, vol. 38, no. 9, pp. 1573–1584, 2015. DOI: 10.2514/1.G001019.

[9] G. Zhang, D. Zhou, D. Mortari, and M. R. Akella, "Covariance analysis of Lambert's problem via Lagrange's transfer-time formulation," *Aerospace Science and Technology*, vol. 77, pp. 765–773, 2018. DOI: 10.1016/j.ast.2018.03.039.

[10] N. Adurthi and M. Majji, "Uncertain Lambert Problem: A Probabilistic Approach," *The Journal of the Astronautical Sciences*, vol. 67, pp. 361–386, 2020. DOI: 10.1007/s40295-019-00205-z.

[11] R. Armellin, P. Di Lizia, F. Topputo, M. Lavagna, F. Bernelli-Zazzera, and M. Berz, "Gravity Assist Space Pruning based on Differential Algebra," *Celestial mechanics and dynamical astronomy*, vol. 106, no. 1, pp. 1–24, 2010. DOI: 10.1007/s10569-009-9235-0.

[12] H.-y. Li, Y.-Z. Luo, G.-J. Tang, *et al.*, "Optimal multi-objective linearized impulsive rendezvous under uncertainty," *Acta Astronautica*, vol. 66, no. 3-4, pp. 439–445, 2010. DOI: 10.1016/j.actaastro.2009.06.019.

[13] Z. Yang, Y.-z. Luo, and J. Zhang, "Robust Planning of Nonlinear Rendezvous with Uncertainty," *Journal of Guidance, Control, and Dynamics*, vol. 40, no. 8, pp. 1954–1967, 2017. DOI: 10.2514/1.G002319.

[14] M. Balducci and B. A. Jones, "Asteroid Rendezvous Maneuver Design Considering Uncertainty," in *Advances in the Astronautical Sciences*, Univelt, Ed., vol. 168, 2019, pp. 2951–2967.

[15] F. Xiong, Y. Xiong, and B. Xue, "Trajectory Optimization under Uncertainty based on Polynomial Chaos Expansion," in *AIAA Guidance, Navigation, and Control Conference*, 2015, p. 1761. DOI: 10.2514/6.2015-1761.

[16] C. Greco, S. Campagnola, and M. L. Vasile, "Robust Space Trajectory Design using Belief Stochastic Optimal Control," in *AIAA Scitech 2020 Forum*, 2020, p. 1471. DOI: 10.2514/6.2020-1471.

[17] N. Ozaki, S. Campagnola, and R. Funase, "Tube stochastic optimal control for nonlinear constrained trajectory optimization problems," *Journal of Guidance, Control, and Dynamics*, 2020. DOI: 10.2514/1.G004363.

[18] N. Marmo, A. Zavoli, N. Ozaki, and Y. Kawakatsu, "A hybrid multiple-shooting approach for covariance control of interplanetary missions with navigation errors," in *33rd AAS/AIAA Space Flight Mechanics Meeting*, Austin, TX, 2023.

[19] B. Benedikter, A. Zavoli, Z. Wang, S. Pizzurro, and E. Cavallini, "Convex approach to covariance control with application to stochastic low-thrust trajectory optimization," *Journal of Guidance, Control, and Dynamics*, vol. 45, no. 11, pp. 2061–2075, 2022. DOI: 10.2514/1.G006806.

[20] J. Ridderhof, P. Tsiotras, and B. J. Johnson, "Stochastic entry guidance," *Journal of Guidance, Control, and Dynamics*, vol. 45, no. 2, pp. 320–334, 2022. DOI: 10.2514/1.G005964.

[21] C. Giordano and F. Topputo, "Analysis, design, and optimization of robust trajectories in cislunar environment for limited-capability spacecraft," *The Journal of the Astronautical Sciences*, vol. 70, no. 6, p. 53, 2023.

[22] P. S. Maybeck, *Stochastic Models, Estimation, and Control*. Academic Press, 1982, vol. 3.

[23] B. Schutz, B. Tapley, and G. H. Born, *Statistical orbit determination*. Elsevier, 2004.

[24] C. Acton, N. Bachman, B. Semenov, and E. Wright, "A look towards the future in the handling of space science mission geometry," *Planetary and Space Science*, vol. 150, pp. 9–12, 2018. DOI: 10.1016/j.pss.2017.02.013.

[25] D. G. Yárnoz, R. Jehn, and M. Croon, "Interplanetary navigation along the low-thrust trajectory of BepiColombo," *Acta Astronautica*, vol. 59, no. 1-5, pp. 284–293, 2006. DOI: 10.1016/j.actaastro.2006.02.028.

[26] S. J. Sheather and J. S. Marron, "Kernel Quantile Estimators," *Journal of the American Statistical Association*, vol. 85, no. 410, pp. 410–416, 1990. DOI: 10.2307/2289777.

[27] R. Walker, D. Koschny, C. Bramanti, *et al.*, "Miniaturised Asteroid Remote Geophysical Observer (M-ARGO): A stand-alone deep space CubeSat system for low-cost science and exploration missions," in *6th Interplanetary CubeSat Workshop, Cambridge, UK*, 2017, pp. 1–20.

[28] A. Mereta and D. Izzo, "Target selection for a small low-thrust mission to near-earth asteroids," *Astrodynamics*, vol. 2, no. 3, pp. 249–263, 2018. DOI: 10.1007/s42064-018-0024-y.

[29] F. Topputo *et al.*, "Envelop of reachable asteroids by M-ARGO CubeSat," *Advances in Space Research*, 2021. DOI: 10.1016/j.asr.2021.02.031.

[30] F. Topputo, D. A. Dei Tos, K. Mani, *et al.*, "Trajectory design in high-fidelity models," in *7th International Conference on Astrodynamics Tools and Techniques (ICATT), Oberpfaffenhofen, Germany*, 2018, pp. 1–9.

[31] V. Franzese *et al.*, "Target Selection for M-ARGO Interplanetary CubeSat," in *71st International Astronautical Congress (IAC 2020)*, 2020, pp. 1–15.

[32] A. Wächter and L. T. Biegler, "On the implementation of an interior-point filter line-search algorithm for large-scale nonlinear programming," *Mathematical programming*, vol. 106, no. 1, pp. 25–57, 2006. DOI: 10.1007/s10107-004-0559-y.

[33] S. Alfano and M. L. Greer, "Determining If Two Solid Ellipsoids Intersect," *Journal of Guidance, Control, and Dynamics*, vol. 26, no. 1, pp. 106–110, 2003. DOI: 10.2514/2.5020.

[34] J. Giorgini and D. Yeomans, "On-line system provides accurate ephemeris and related data," NASA, Tech. Rep., 1999.